MULTI-MODE GVT/FEM CORRELATION

S. Siegel and V. K. Gupta

Members of the Technical Staff
North American Aircraft
Rockwell International Corporation
El Segundo, California, U.S.A.

1.0 Abstract

A practical optimization method for adjusting each element stiffness of a finite element structural model (FEM) has been developed to improve the correlation of both frequencies and mode shapes predicted by the FEM with those measured by the ground vibration test (GVT). A modified version of the Van de Vooren perturbation technique is developed to effectively approximate (1) frequency and mode shape derivatives of each finite element or each preselected substructure (group of elements) and (2) the eigensolutions. The derivatives are used to determine element stiffness factors for a gradient search algorithm to modify the structure within reasonable bounds to converge in incremental steps to achieve an acceptable correlation. The eigenvalue solution with the modified FEM verifies the convergence. A NASTRAN-based FEM of a wing torque box, using nine modes, demonstrates the cost effectiveness, efficiency, reliability, and accuracy of the method.

2.0 Introduction

During the course of developing a structural system, the FEM is usually constructed to analyze the system dynamic characteristics. On the basis of the calculated dynamic and static characteristics, the structure is determined to be adequate, marginal, or inadequate to meet the required specifications, such as preventing flutter and divergence from occurring within the flight envelope. If found to be inadequate, the structure is modified to be at least marginal. Most dynamic analyses, in general, yield approximate solutions based on overly conservative assumptions such that the resulting solution characteristics may be doubtful as to their accuracy. For these doubtful solutions, specially when found to be marginal, natural mode testing is required to validate the structural dynamic basis for the analysis.

As usually happens, the test frequencies and mode shapes differ from those calculated. Several methods found in the current literature have been proposed to achieve modal correlation between analysis and test. Many of these methods (1-6) modify the analytical stiffness and mass matrices. While some of the methods apparently improve correlation with the test modes in essentially closed form, the modified stiffness and mass matrices are not traceable to reflect the actual structural modification. Sometimes a strain energy density approach or detuning has been used to avoid resonant vibrations (10).

In contrast to such matrix adjustment methods, this paper describes a method whereby the structural modifications can be assessed at the FEM level to achieve improved correlation. The proposed Multi-Mode GVT/FEM Correlation method of modifying structural elements, rather than the stiffness matrix, tends to be more meaningful to the analysts, designers, and manufacturers. Based on the adjusted and correlated structure and the validated FEM, more accurate and reliable solutions for the dynamic-characteristics of that structure will yield greater confidence in the integrity of the structure.

3.0 Description of Method

The Ground Vibration Test/Finite Element Model (GVT/FEM) Correlation method and code (NCP) of this paper combines the general-purpose finite-element structural analyses capabilities of NASTRAN (7) with a new external program, CORFEM. CORFEM compares the analytical (FEM) modes with the test (GVT) modes in order to optimize the adjustments to the FEM. The mass matrix is assumed to be unchanged and the modes to have little or no damping. Also, since modal testing is performed with some kind of structural support for the test vehicle, only fixed-free and fixed-fixed boundary conditions, including soft suspension supports, are considered.

The essential feature in CORFEM is the modified version of the Van de Vooren perturbation method (MVP), that efficiently calculates the new frequencies and mode shapes of a given structure for perturbations to the stiffness and mass properties of the structure (8). The modification uses a recursive technique that is amenable to the modern computer that was not previously available.

Recursive 1 retains the first order and implicitly updates frequency and mode shapes; recursive 2, retains the first order and updates eigenvalues and eigenvectors explicitly, as indicated by the equations in Appendix C. Table 1 shows how convergence of the eigenvalues (roots) for the original Van de Vooren formulae compare with those of the modified recursive versions for a two degree of freedom problem.

The flow chart of Figure 1 indicates the essential steps in two loops for the overall program. During the iterative inner loop, after the analytical modes have been calculated and determined to exceed the correlation tolerance, the changes in element stiffnesses are calculated using the frequency and mode shape derivatives based on the MVP technique. The new frequencies and mode shapes for the updated structure are also calculated using MVP. In the outer loop, the FEM is updated through NASTRAN and an exact eigensolution is obtained to verify the MVP solution. The process is repeated until the

correlation tolerance is met. As shown in Figure 1, the procedure takes the following steps:

(1) NASTRAN generates the FEM and the flexibility, mass, and element stiffness matrices in the dynamic degrees of freedom (DDOF).

(2) CORFEM calculates the FEM modes and sorts them to correspond with the GVT modes.

(3) CORFEM computes for each selected mode the square root sum of squares (SRSS) of frequency and mode shape errors and the total error between corresponding or matching FEM and GVT modes.

(4) Convergence within CORFEM occurs if the total error is less than the required tolerance, or if a local SRSS minimum occurs.

(5) Until convergence occurs, FEM frequency and mode shape derivatives and element siffness change factors are updated, based on a constrained optimization method.

TABLE 1. ROOT ERROR COMPARISON BETWEEN ORIGINAL AND RECURSIVE VAN DE VOOREN METHODS FOR TWO DOF PROBLEMS

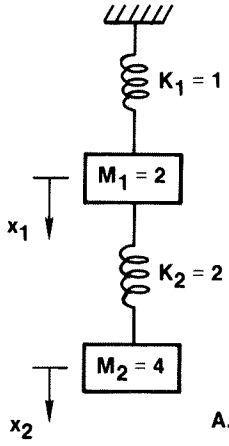

A. TWO DOF FEM

PER CENT ROOT ERRORS FOR $K_1 = 2$

METHOD	ROOT NO.	APPROXIMATION ORDER 1	2	3	4
ORIGINAL	1	-8.52	0.09	—	—
	2	0.90	-0.01	—	—
RECURSIVE 1	1	-8.52	0.65	-0.05	+0.00
	2	0.90	-0.02	+0.00	0.00
RECURSIVE 2	1	-8.52	0.09	—	—
	2	0.90	-0.01	—	—

B. ROOT ERROR CHART

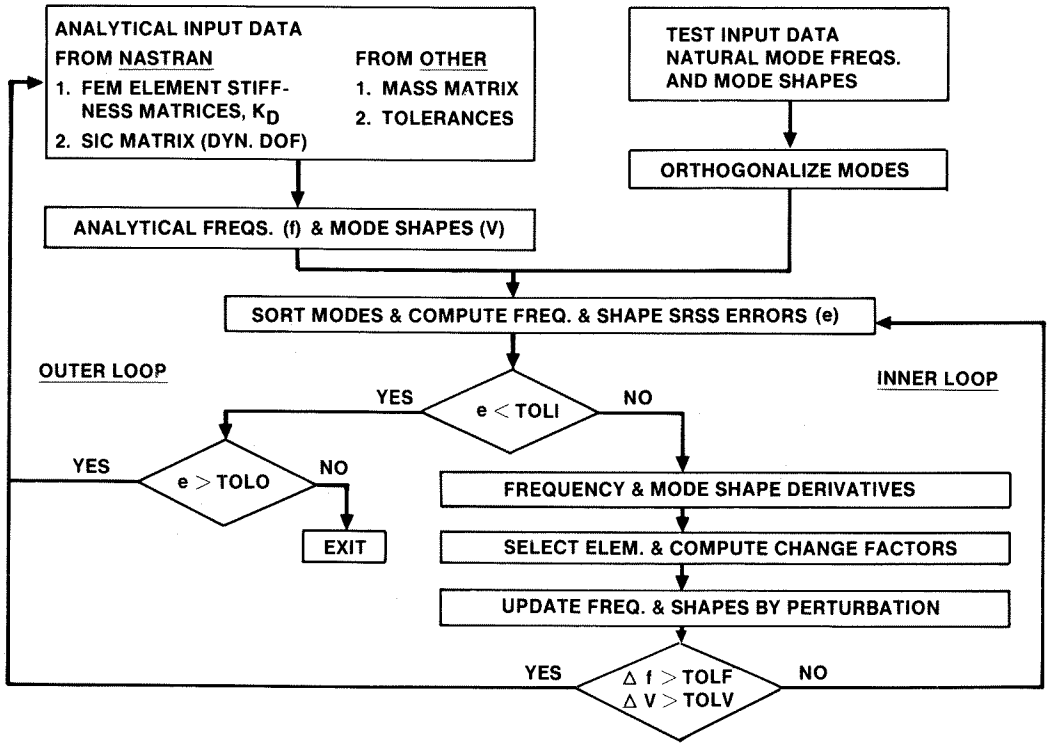

Figure 1. Flow Chart of GVT/FEM Correlation

3.1 NASTRAN Finite Element Analysis (Outer Loop)

A finite element model of the given structural design is formulated and constructed for analysis with Rockwell's version of the NASA COSMIC-released NASTRAN [7] software program. Multipoint constraint equations (MPC) are separately generated using a preprocessor for Rockwell NASTRAN that couples user-selected points, associated with the DDOF and which are identical to the GVT DOF, to the structural DOF (SDOF). NASTRAN is used to generate the flexibility matrix and to transform it from SDOF to DDOF using the MPC-based transformation (T) as follows:

$$K_D^{-1} = T^t K_S^{-1} T \qquad (1)$$

The transformation matrix (B) relating the DDOF to the SDOF, as derived in Appendix A, is obtained with a NASTRAN DMAP instruction:

$$B = K_D T^t K_S^{-1} \qquad (2)$$

The current CORFEM program calculates the FEM modes using the DDOF. Since the deformations of the GVT mode shapes are normally restricted to a reasonable number of points and DOF on the vibrating structure, a maximum of about 200 DOF, the analytical model is transformed to these DDOF. This one-to-one correspondence between the FEM and GVT modes can provide an on line solution to obtain information for making timely engineering judgments concerning the structure. The inner loop iterative process of Figure 1 uses a further DOF reduction, the modal DOF, which reduces the order of the eigenvalue problem for rapid optimization.

3.2. Orthogonalization of Test Modes

For proper correlation, the GVT modes should be orthogonal with respect to the mass matrix, under the assumption that the mass matrix is valid for the structural system of the test. A procedure to orthogonalize the modes is given in Appendix B. This orthogonalization should be preceded by careful observation of the modes shapes in an attempt to smooth the data using engineering judgment based on test-mode-shape plots. If after the orthogonalization process, some of the modal frequencies and shapes deviate significantly from the raw data, then those deviant modes should be deleted from the correlation process. The degree of deviation warranting deletion is a question of engineering judgment. These deleted modes may be presumed to have been measured inaccurately. The remaining modes should be suitable for correlation.

3.3 CORFEM Optimization (Inner Loop)

3.3.1 Mode Sorting. A one-to-one correspondence between the FEM and GVT modes is required to obtain the appropriate SRSS errors based on sorting the scaled FEM modes with respect to the scaled GVT modes, as respectively denoted using subscripts F and G. Scaled modes are defined to be mass-orthonormal:

$$(V_F)^t M (V_F) = I \quad \text{and} \quad (V_G)^t M (V_G) = I \qquad (3)$$

The sorting criteria uses a cross-orthogonalization between the FEM and GVT modes. The ith FEM mode corresponds to the jth GVT mode where m_{ij} is closest to unity.

$$(V_F)_i^t M (V_G)_j = m_{ij} \qquad (4)$$

If a higher frequency ith mode selects the same jth mode, then the modes are sorted according to the mode closest to the value of unity.

3.3.2 Objective Function (SRSS Errors). After matching the FEM modes with the corresponding GVT modes, the SRSS error in frequencies and mode shapes is calculated as follows:

$$e_f = \left[\sum_{i=1}^{n} (f_F - f_G)^2\right]^{1/2} \qquad (5)$$

$$e_V = \left[\sum_{i=1}^{n}\sum_{j=1}^{d} (V_F - V_G)^2 / d\right]^{1/2} \qquad (6)$$

where d = number of DDOF
n = selected number of modes

Convergence to a global minimum occurs when the error sum $e_S = e_f + e_V$, becomes less than a required tolerance of approximately 2%.

3.3.3 Frequency and Mode Shape Error Derivatives. To minimize the error sum, a constrained optimization procedure determines adjustment factors for the element stiffnesses using the frequency and mode shape derivatives. The modified Van de Vooren formulae for updating frequencies and mode shapes due to the stiffness perturbation, ΔK, as derived in Appendix C, for Recursive 1, are:

$$(\Delta\lambda)_{i\,r} = -(k_{ii} + \beta_{ii})^{-1} \left[\beta_{ii}\lambda_i + (\lambda)_{i\rho}\sum_{j=1}^{n}\beta_{ij}(p_{ji})_\rho\right] \quad i\neq j \qquad (7)$$

$$\left.\begin{aligned} p_{ii} &= 1.0 \\ (p_{ij})_r &= \\ &-\left[\beta_{ij} + \sum_{s=1}^{n}\beta_{is}(p_{sj})_\rho\right]\Big/\left[k_{ii} + \beta_{ii} - (\lambda)_{i\,r}^{-1}\right] \quad s\neq i\&j;\ i\neq j \end{aligned}\right\} \qquad (8)$$

$$\Delta V = V\,(p-1) \qquad (9)$$

where $\beta = V^t(\Delta K)\,V$

k_{ii} = diagonal elements of $V^t K V$
K = dynamic stiffness matrix
ΔK = change in dynamic stiffness matrix
V = dynamic mode shapes
$\lambda_i = \omega_i^{-2} = (2\pi f_i)^{-2}$
p_{ij} = generalized mode shape
r = order of approximation
ρ = r-1
n = number of system modes

The frequencies and mode shapes for a small stiffness change of each element may alternately be expressed as follows:

$$f_F = (1/2\pi)\left[\lambda + (\Delta\lambda)\right]^{-1/2} \quad (10)$$

$$V_F = V_r p \quad (11)$$

The change in SRSS error sum due to 0.1% change, say, in each element stiffness matrix is used to compute derivative or modal sensitivity due to that element:

$$\Delta e/\Delta k = (e_f + e_V - e_S)/\Delta k \quad (12)$$

where Δk = the change in the generalized stiffness for the given element

3.3.4 Computation of Stiffness Change Factors. The stiffness matrix of a selected element or substructure is multiplied by its factor c that is optimally determined to minimize the SRSS error sum by performing a gradient search such that the elements with the larger derivatives obtain the larger c values in a given iteration.

$$(c)_i = R\, e_S\, (\Delta e/\Delta k)_i \quad (13)$$

where R ≈ 0.8 for the first iteration
R ≈ 1.0 for subsequent iterations

These c values are restricted to within reasonable bounds, say, a minimum of 0.55 and maximum of 1.50.

3.3.5 Update of Frequencies and Mode Shapes by MVP. After the stiffness change factors are updated, the element stiffness matrices are summed to obtain the total system stiffness matrix in DDOF; and the new frequencies and mode shapes are calculated via the recursive Van de Vooren formulas using Eqs. (7)-(9).

3.3.6 Convergence Criteria. Convergence is deemed to occur when the following conditions are satisfied; otherwise, the inner loop of steps (2) through (5) of paragraph 3.0 are repeated.

(i) the SRSS error sum reaches a local minimum,

(ii) the SRSS error sum meets the inner loop tolerance (TOLI), or exceeds the frequency, mode shape, and outer loop tolerances (TOLF, TOLV, TOLO of Figure 1).

If tolerances are exceeded, the FEM is modified to the current update of the inner loop and the NASTRAN FEM analysis of the outer loop is executed. This outer-inner loop process is repeated until the SRSS error sum is within the designated inner and outer loop tolerances. Once the outer loop set of analytical modes meets the designated tolerance requirements, the modes are considered correlated and the program is exited.

4.0 Illustrative Examples

4.1 Introduction

The examples presented here are based on an all aluminum wing torque box shown in Figure 2 by a quasi-isometric view. The 16 circled points represent the structural nodes having x, y, and z displacements. Structural nodes 13, 14, 15, and 16 are fixed. The nine square points are the dynamic nodes having z displacements only. The dynamic nodes are assumed to be in the mid-wing plane. Figure 3 shows the distribution of the finite elements consisting of upper and lower cover elements, vertically oriented shear elements, and rod elements.

Four different FEM cases were generated to exercise the NASTRAN/CORFEM software programs (NCP). Table 2 shows the structural node points and gages for the rod, shear, and membrane elements for the cases. Case 1 FEM incorporated 15 trapezoidal shear elements cornered by four structural nodes and 24 rod elements with two structural nodes, one node at each end of each rod. Each rod element had a cross section of 0.20 sq. in.; and each shear element had a gage of 0.01 in. for the GVT configuration and a gage of 0.015 in. for the FEM configuration.

Cases 2, 3, and 4 were built from six membrane elements, three for the upper cover and three for the lower cover, nine shear elements for the "ribs" and "spars," and 24 rod elements. The GVT configuration for the three cases had shear and membrane elements with gages of 0.010 in. and rod element areas of 0.01 sq. in. and shear and membrane gages of 0.015 in. Case 3 FEM had rod membrane gages of 0.01 sq. in. and shear and membrane elements with alternating gages of 0.013 and 0.007 in., as shown in Table 2.

Case 4 FEM had rod areas of 0.010 sq. in. and shear and membrane gages of 0.010 in. except for element 8, which had a gage of 0.0001 in. The anomalous gage for element 8 was selected to represent a possible inadvertent error by the FEM modeler.

Two basic assumptions were applied for the four cases. The dynamic mass matrix, which consisted of non-zero elements on the diagonals only, remained unchanged; and only the shear and membrane elements were allowed to change gage during the correlation. Comparisons of the upper and lower cover gages between the GVT and the FEM cases are shown in Figure 4.

4.2 Case 1 Results

Case 1 was selected initially as a convenient problem for NCP to solve. The GVT frequencies and the FEM frequencies with their percent errors are listed in Table 3. Modes 2, 4, 5, and 7 reflect errors associated with the shear element stiffnesses. Modes 1, 6, 8, and 9 were dominated by the rod element stiffnesses, which were the same in the FEM as for the GVT configuration, as indicated by the small

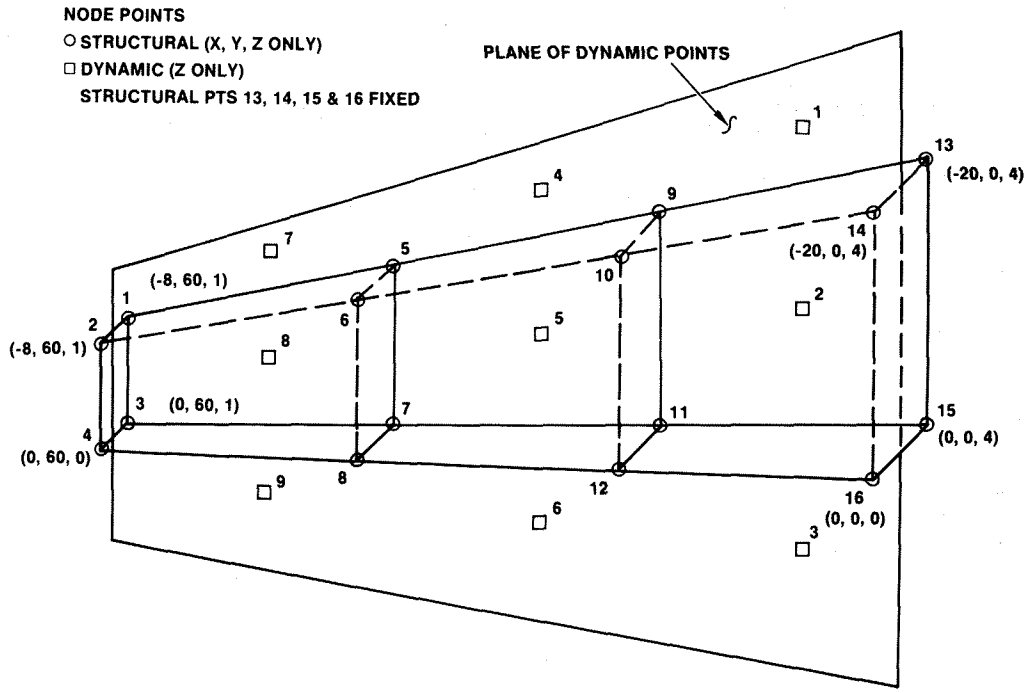

Figure 2. FEM Test Case Node Points

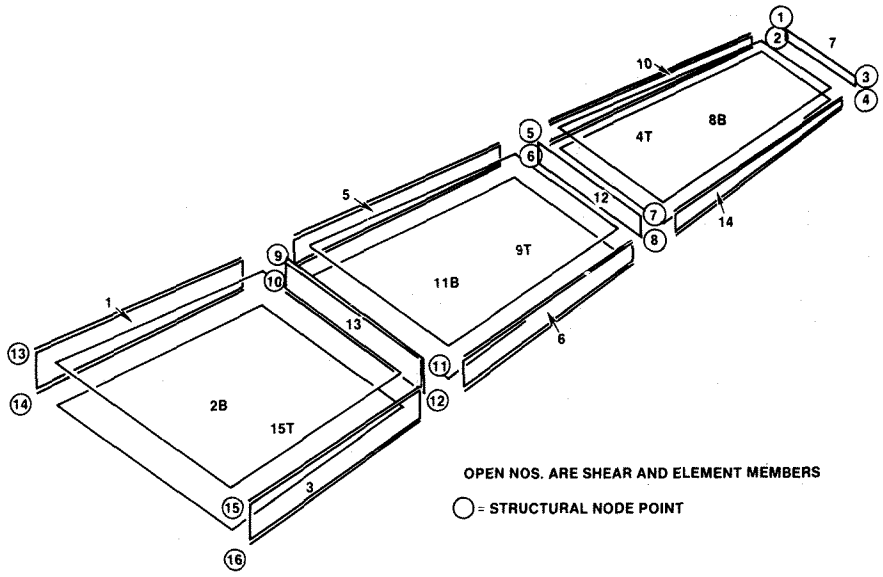

Figure 3. FEM Structural Elements

TABLE 2. WING TORQUE BOX FEM ELEMENT DEFINITIONS AND GAGES

ELEM NO.	STRUCT. NODE PTS.				CASE 1		CASE 2		CASE 3		CASE 4	
					TYPE	GAGE, IN.	TYPE	GAGE, IN.	TYPE	GAGE, IN.	TYPE	GAGE, IN.
1	14	10	9	13	S	0.015	S	0.015	S	0.013	S	0.010
2	10	12	16	14	S	0.015	M	0.015	M	0.007	M	0.010
3	16	12	11	15	S	0.015	S	0.015	S	0.013	S	0.010
4	1	3	7	5	S	0.015	M	0.015	M	0.007	M	0.010
5	10	6	5	9	S	0.015	S	0.015	S	0.013	S	0.010
6	12	8	7	11	S	0.015	S	0.015	S	0.007	S	0.010
7	2	4	3	1	S	0.015	S	0.015	S	0.013	S	0.010
8	2	4	8	6	S	0.015	M	0.015	M	0.007	M	0.0001
9	5	7	11	9	S	0.015	M	0.015	M	0.013	M	0.010
10	6	2	1	5	S	0.015	S	0.015	S	0.007	S	0.010
11	6	8	12	10	S	0.015	M	0.015	M	0.013	M	0.010
12	6	8	7	5	S	0.015	S	0.015	S	0.007	S	0.010
13	10	12	11	9	S	0.015	S	0.015	S	0.013	S	0.010
14	8	4	3	7	S	0.015	S	0.015	S	0.007	S	0.010
15	9	11	15	13	S	0.015	M	0.015	M	0.013	M	0.010
16-39					ROD	0.20	ROD	0.010	ROD	0.010	ROD	0.010

S = SHEAR ELEMENT M = MEMBRANE ELEMENT

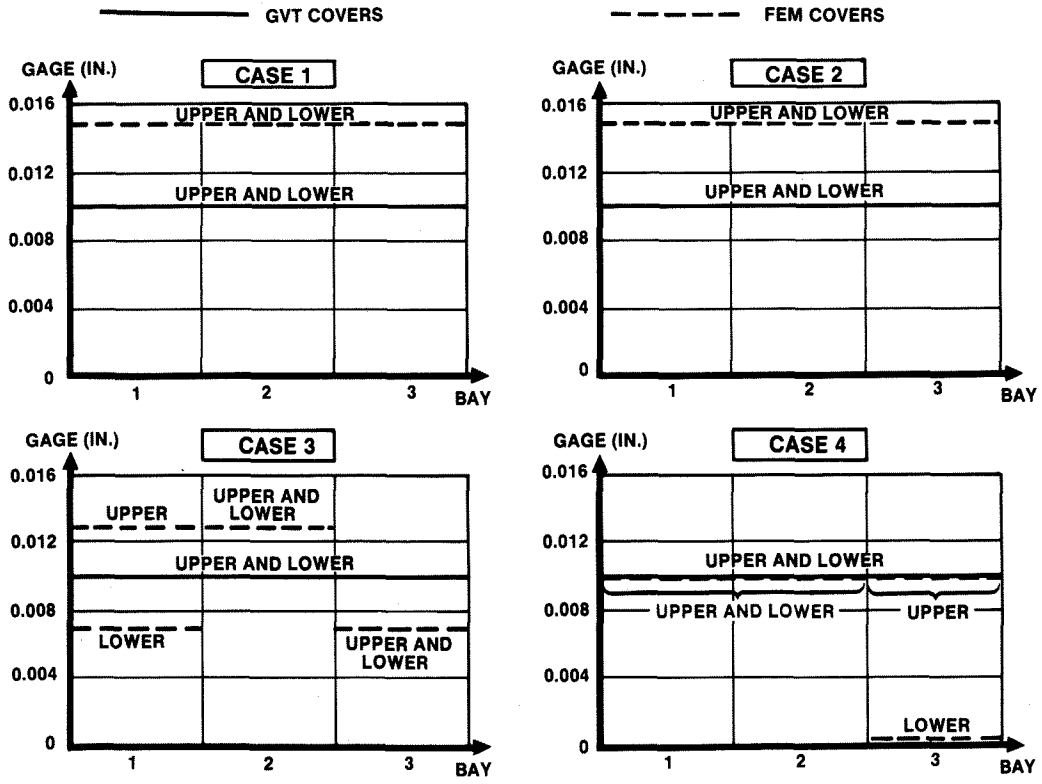

Figure 4. Cover Gages for Cases 1, 2, 3, and 4

TABLE 3. FREQUENCY AND PERCENT ERROR CHANGES FOR CASE 1

MODE NO.	GVT FREQ, HZ	INITIAL FEM		PASS 1		PASS 2	
		FREQ, HZ	% ERROR	FREQ, HZ	% ERROR	FREQ, HZ	% ERROR
1	10.66	10.79	1.2	10.66	0.0	10.65	-0.1
2	28.50	34.06	19.5	28.42	-0.3	28.43	-0.2
3	47.00	51.70	10.0	47.36	0.8	47.03	0.1
4	80.58	96.64	19.9	80.57	-0.0	80.49	0.1
5	186.3	216.7	16.3	185.0	-0.7	184.7	-0.9
6	247.1	250.7	1.5	247.0	-0.0	247.1	0.0
7	298.8	350.5	17.3	296.1	-0.9	296.5	-0.8
8	461.5	477.5	3.5	461.1	-0.1	461.2	-0.1
9	2656.	2729.	2.7	2677.	-0.8	2673.	0.6
FREQ. RMS ERROR		12.76%		0.54%		0.45%	
SHAPE RMS ERROR		7.67%		1.08%		0.54%	

percentage frequency errors. The plots of Figure 5 show the frequency and mode shape error convergence for the two passes of NCP. The initial SRSS frequency and mode shape errors, as shown in Figure 5, were 0.3828 and 0.2361, or 38.28% and 23.61%; the equivalent RMS errors were 12.76% and 7.67% The first pass through NCP showed a significant reduction in both the frequency and mode shape errors, particularly for the first three iterations. The remaining four iterations of the first pass achieved further error reductions but by smaller factors to eventually meet the tolerance SRSS value of 2.5%. An analysis update of the FEM through NASTRAN was performed, and the second pass inner loop iterations met a tolerance SRSS value of 1.5%. The final check yielded very small RMS errors of 0.45% for frequencies and 0.54% for mode shapes. RMS errors are tabulated because of its popular usage. Comparisons of the node lines are shown in Figure 6. Relatively small differences appeared between the GVT and the initial FEM node lines, except for mode 8. The correlated node lines were almost identical for all nine modes.

The shear element gage errors are listed in Table 4, showing the initial FEM gages with RMS errors of 50%. These gage errors were reduced by NCP to an RMS error of 7.0% after pass 1 and to 3.9% after pass 2.

The updated finite element eigensolution analysis check yielded a slightly different set of frequencies and mode shape errors than those at the end of the MVP pass 1. This difference is attributed to a combinaton of the approximate nature of the perturbation solution and the update of the transformation matrix, B, by the NASTRAN second analysis.

The results of Case 1 were considered well within the realm of engineering accuracy to pursue other cases to develop more experience with NCP.

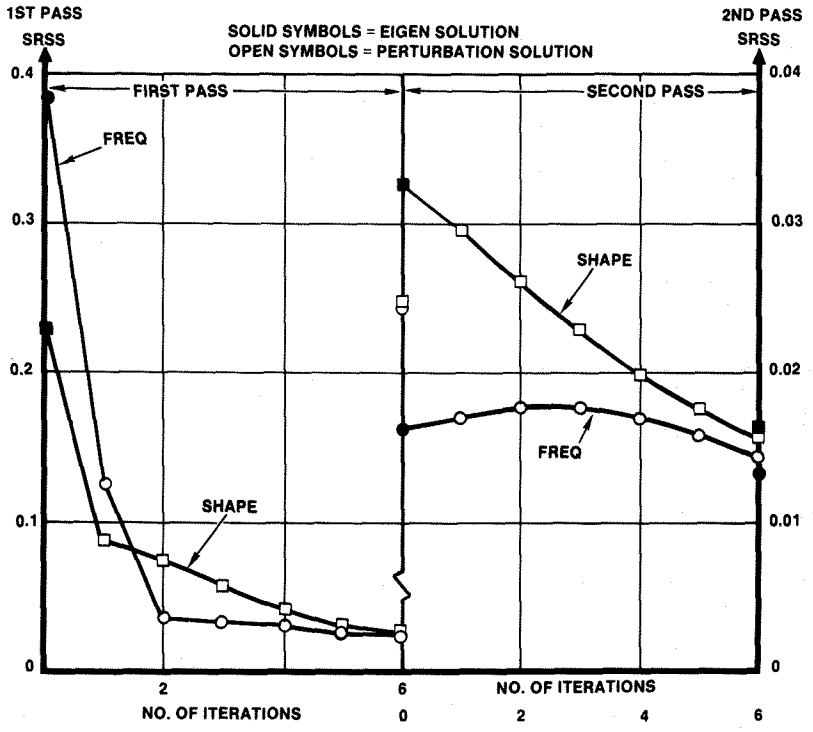

Figure 5. SRSS Errors With Iteration for Case 1

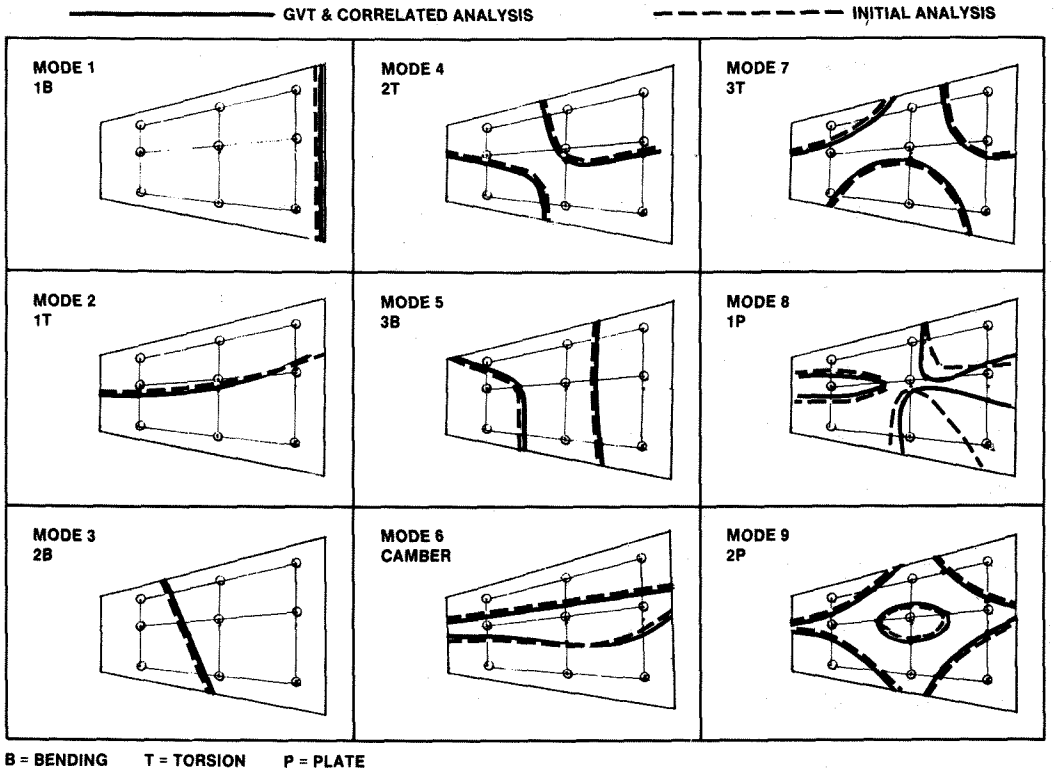

Figure 6. GVT and FEM Node Line Comparisons for 9 Modes (Case 1)

TABLE 4. GAGE AND PERCENT ERROR CHANGES FOR CASE 1

ELEM NO.	TYPE	GVT GAGE, IN.	INITIAL FEM		PASS 1		PASS 2	
			GAGE, IN.	% ERROR	GAGE, IN.	% ERROR	GAGE, IN.	% ERROR
1	S	0.010	0.0150	50.0	0.01063	6.3	0.01018	1.8
2	S	0.010	0.0150	50.0	0.01147	14.7	0.01083	8.3
3	S	0.010	0.0150	50.0	0.01038	3.8	0.00999	-0.1
4	S	0.010	0.0150	50.0	0.01092	9.2	0.01066	6.6
5	S	0.010	0.0150	50.0	0.00952	-4.8	0.00947	-5.3
6	S	0.010	0.0150	50.0	0.00950	-5.0	0.00964	-3.6
7	S	0.010	0.0150	50.0	0.01018	1.8	0.01007	0.7
8	S	0.010	0.0150	50.0	0.00937	-6.3	0.00957	-4.3
9	S	0.010	0.0150	50.0	0.00949	-5.1	0.00977	-2.3
10	S	0.010	0.0150	50.0	0.00928	-7.2	0.00958	-4.2
11	S	0.010	0.0150	50.0	0.00924	-7.6	0.00966	-3.4
12	S	0.010	0.0150	50.0	0.00952	-4.8	0.00987	-1.3
13	S	0.010	0.0150	50.0	0.00957	-4.3	0.00993	-0.7
14	S	0.010	0.0150	50.0	0.00926	-7.4	0.00977	-2.3
15	S	0.010	0.0150	50.0	0.00923	-7.7	0.00965	-3.5
SHEAR ELEM RMS ERROR			50.0%		7.0%		3.9%	

NOTE: S = SHEAR ELEMENT

4.3 Case 2 Results

The FEM for Case 2 reflected a more normal wing torque box structure by using membranes instead of shear elements for the covers and more flexible rods with reduced cross sectional areas than for Case 1. See Table 2. Since the membrane elements now dominated the box stiffness, the constant gages of 0.01 in. for the GVT and 0.015 in. for the FEM yielded constant RMS frequency errors of approximately 21% between the GVT modes and the initial FEM modes, as indicated in Table 5. The mode shape errors were relatively small. For both passes 1 and 2 of NCP, most of the frequency error reductions occurred during the first three inner loop iterations, as indicated in the converging plots of Figure 7. The results of pass 1 reduced the RMS frequency error from 21.1% down to 2.2% and for pass 2 down to 0.4%. Table 5 shows the frequency errors of the nine modes for the initial FEM and after the two passes. Similarly, the mode shape RMS error dropped from 0.83% to 0.77% to 0.48%.

The gage correlations between GVT and FEM, as shown in Table 6, indicated that the membrane elements had an initial RMS error of 50%, which was reduced to 6.7% after pass 2. Since some of the shear elements did not significantly affect the modes, their gage RMS errors were reduced from the initial value of 50.% down to 27.3%. The frequency and mode shape errors were significantly reduced by a second pass while the gage errors did not change much, except in distribution.

The correlation results of Case 2, for which two kinds of elements were allowed to vary, were also considered within engineering accuracy. They showed NCP to yield successful results for dynamic analysis usage.

4.4 Case 3 Results

The initial FEM shear and membrane element gages were chosen to alternate from 0.013 in. to 0.007 in., as indicated in Table 2 and in Figure 4, which show the membrane elements only. This case was analyzed to exercise NCP for a more stringent example. The gages were allowed to range between a minimum of 0.007 in. and a maximum of 0.013 in. Three passes were calculated, and Figure 8 shows the convergence trends for the frequency and mode shape errors. Starting with RMS frequency and mode shape errors of 5.0% and 8.9%, the RMS errors after pass 3 were reduced to 0.4% and 1.3%.

TABLE 5. FREQUENCY AND PERCENT ERROR CHANGES FOR CASE 2

MODE NO.	GVT FREQ, HZ	INITIAL FEM		PASS 1		PASS 2	
		FREQ, HZ	% ERROR	FREQ, HZ	% ERROR	FREQ, HZ	% ERROR
1	7.562	9.097	20.3	7.665	1.4	7.551	-0.1
2	26.79	32.68	22.0	27.38	2.2	26.80	0.0
3	36.09	43.59	20.8	36.82	2.1	36.12	0.1
4	77.64	94.74	22.0	79.47	2.4	77.80	0.2
5	156.6	189.9	21.3	161.1	2.9	156.8	0.1
6	241.4	293.2	21.5	247.2	2.4	242.7	0.5
7	278.5	338.9	21.7	286.2	2.8	279.9	0.5
8	392.7	475.8	21.2	399.1	1.6	391.3	-0.4
9	1533.	1826.	19.1	1546.	0.8	1520.	-0.8
FREQ. RMS ERROR		21.11%		2.15%		0.42%	
SHAPE RMS ERROR		0.83%		0.77%		0.48%	

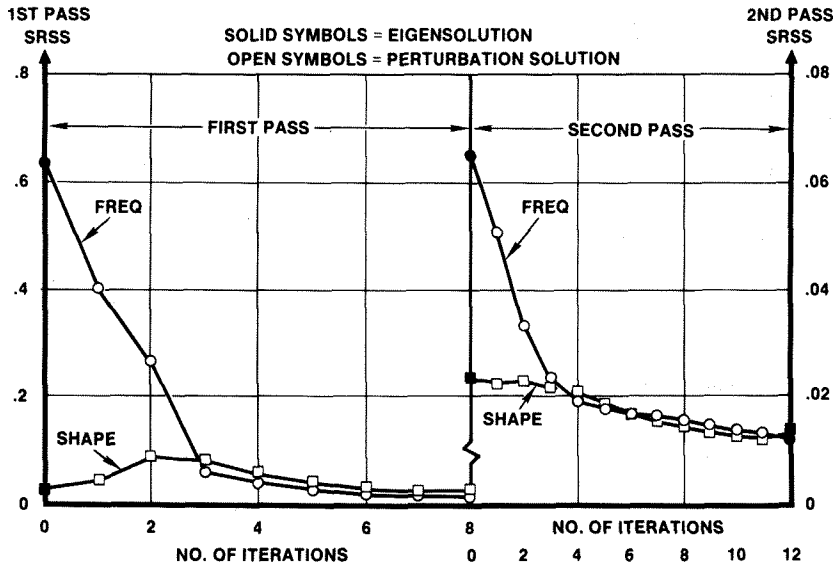

Figure 7. SRSS Errors With Iteration for Case 2

TABLE 6. GAGE AND PERCENT ERROR CHANGES FOR CASE 2

ELEM NO.	TYPE	GVT GAGE	INITIAL FEM		PASS 1		PASS 2	
			GAGE	% ERROR	GAGE	% ERROR	GAGE	% ERROR
1	S	0.010	0.0150	50.0	0.01051	5.1	0.01017	1.7
2	M	0.010	0.0150	50.0	0.00951	-4.9	0.00922	- 7.8
3	S	0.010	0.0150	50.0	0.01087	8.7	0.01010	1.0
4	M	0.010	0.0150	50.0	0.01060	6.0	0.01039	3.9
5	S	0.010	0.0150	50.0	0.01105	10.5	0.01006	0.6
6	S	0.010	0.0150	50.0	0.01080	8.0	0.00982	- 1.8
7	S	0.010	0.0150	50.0	0.01200	12.0	0.01114	11.4
8	M	0.010	0.0150	50.0	0.00956	-4.4	0.00900	-10.0
9	M	0.010	0.0150	50.0	0.01013	1.3	0.00949	- 5.1
10	S	0.010	0.0150	50.0	0.01339	33.9	0.01291	29.1
11	M	0.010	0.0150	50.0	0.01077	7.7	0.01047	4.7
12	S	0.010	0.0150	50.0	0.01445	44.5	0.01456	45.6
13	S	0.010	0.0150	50.0	0.01456	45.6	0.01464	46.4
14	S	0.010	0.0150	50.0	0.01400	40.0	0.01389	38.9
15	M	0.010	0.0150	50.0	0.01116	11.6	0.01082	8.2
SHEAR ELEM RMS ERROR				50.0%		27.8%		27.3%
MEMB ELEM RMS ERROR				50.0%		6.8%		6.7%

NOTE: S = SHEAR ELEMENT M = MEMBRANE ELEMENT

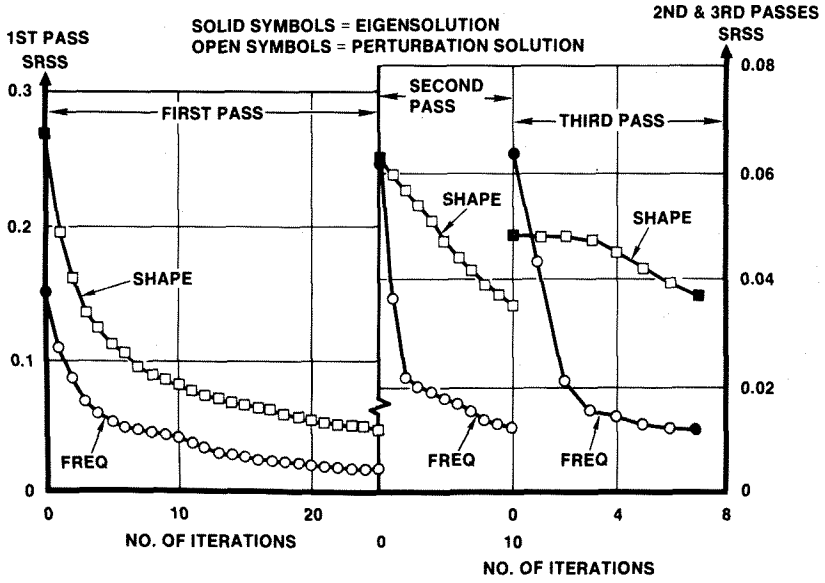

Figure 8. SRSS Errors With Iteration for Case 3

Table 7 shows the frequency errors for all nine modes for the three passes. The eigensolution check after pass 2 shows a higher error than the MVP results, but pass 3 converged back to the MVP result.

The RMS gage errors, shown in Table 8, decreased from the initial value of 30.0% for both shear and membrane elements down to values of 16.5% and 16.0% after three passes. Slight error increases were analyzed after pass 2, which parallels the frequency error increase. Once again the shear elements exhibited relatively large gage errors. A third pass helped to significantly reduce the frequency errors while only slightly changing the gage errors. The gage error redistribution permitted a reduction in the frequency errors. Even for this stringent case, significant improvement in correlating the frequencies and mode shapes resulted from the NCP optimization.

4.5 Case 4 Results

Only one element of the FEM was chosen to reflect an inadvertent modeling error. The outboard bottom cover membrane element was reduced to a gage value of 0.0001 in. with all other elements having a gage value of 0.01 in. After the first iteration, the program calculated a stiffness change factor for this anomalous element that far exceeded any reasonable maximum allowable change. The change factor was calculated to be a value of 60., while the not-to-exceed value was selected as 1.5. As a result of this finding, the NCP may conceivably be used as a tool to detect some of the significant modeling errors.

TABLE 7. FREQUENCY AND PERCENT ERROR CHANGES FOR CASE 3

MODE NO.	GVT FREQ, HZ	INITIAL FEM		PASS 1		PASS 2		PASS 3	
		FREQ, HZ	% ERROR	FREQ, HZ	% ERROR	FREQ, HZ	% ERROR	FREQ, HZ	% ERROR
1	7.562	7.550	-0.2	7.419	-1.9	7.705	1.9	7.590	0.3
2	26.79	28.01	4.5	26.59	-0.7	27.25	1.7	26.78	-0.0
3	36.09	37.07	2.7	35.79	-0.8	36.42	0.9	35.87	-0.6
4	77.64	74.11	-4.5	76.85	-1.0	78.88	1.6	77.15	-0.6
5	156.6	152.0	-2.9	154.5	-1.3	160.9	2.7	156.1	-0.3
6	241.4	255.7	5.9	244.0	1.1	242.6	0.5	240.3	-0.5
7	278.5	268.5	-3.6	275.7	-1.0	285.4	2.5	278.0	-0.2
8	392.7	371.6	-4.4	390.6	-0.5	401.6	2.3	391.9	-0.2
9	1533.	1387.	-9.5	1505.	-1.8	1586.	3.5	1540.	0.5
FREQ RMS ERROR		5.01%		0.74%		2.14%		0.41%	
SHAPE RMS ERROR		8.94%		1.90%		1.61%		1.25%	

TABLE 8. GAGE AND PERCENT ERROR CHANGES FOR CASE 3

ELEM NO.	TYPE	GVT GAGE	INITIAL FEM		PASS 1		PASS 2		PASS 3	
			GAGE	% ERROR	GAGE	% ERROR	GAGE	% ERROR	GAGE	% ERROR
1	S	0.010	0.013	30.0	0.00915	- 8.5	0.00971	- 2.9	0.00958	- 4.2
2	M	0.010	0.007	-30.0	0.00780	-22.0	0.00901	- 9.9	0.00843	-15.7
3	S	0.010	0.013	30.0	0.00990	- 1.0	0.01083	8.3	0.00997	- 0.3
4	M	0.010	0.007	-30.0	0.00949	- 5.1	0.01057	5.7	0.00972	- 2.8
5	S	0.010	0.013	30.0	0.01251	25.1	0.01300	30.0	0.01167	16.7
6	S	0.010	0.007	-30.0	0.01007	0.7	0.01077	7.7	0.00993	- 0.7
7	S	0.010	0.013	30.0	0.01299	29.9	0.01300	30.0	0.01207	20.7
8	M	0.010	0.007	-30.0	0.01049	4.9	0.01132	13.2	0.01046	4.6
9	M	0.010	0.013	30.0	0.01204	20.4	0.01183	18.3	0.01171	17.1
10	S	0.010	0.007	-30.0	0.00912	- 8.8	0.00917	- 8.3	0.00894	-10.6
11	M	0.010	0.013	30.0	0.00912	- 8.8	0.00837	-16.3	0.00845	-15.5
12	S	0.010	0.007	-30.0	0.00700	-30.0	0.00700	-30.0	0.00710	-29.0
13	S	0.010	0.013	30.0	0.01088	8.8	0.00998	- 0.2	0.01010	1.0
14	S	0.010	0.007	-30.0	0.00700	-30.0	0.00700	-30.0	0.00720	-28.0
15	M	0.010	0.013	30.0	0.01256	25.6	0.01286	28.6	0.01270	27.0
SHEAR ELEM RMS ERROR			30%		19.9%		20.6%		16.5%	
MEMB ELEM RMS ERROR			30%		16.7%		16.9%		16.0%	

NOTE: S = SHEAR ELEMENT M = MEMBRANE ELEMENT

4.6 Correlation Using Fewer Number of Modes

The effects of reducing the number of GVT modes from nine to seven, five and three were evaluated for a pass 1 only using Case 2 FEM. Three different number of FEM modes were used: five, seven, and the complete set of nine. For five GVT modes and five, seven, and nine FEM modes, the frequency and percent error changes are shown in Table 9 along with the frequency and mode shape RMS errors and the number of iterations. Similar reduced errors were calculated for the three sets of modes, but the number of iterations required reduced from 30 to 17 to nine as the number of modes increased from five to seven to nine.

Element gage RMS errors tended to be less with an increased number of test modes and very little error change occurred by increasing the number of FEM modes used in the analysis. The frequency and mode shape RMS errors were relatively constant with the number of test modes and the number of analytical modes. See Tables 10, 11, and 12.

5.0 Consideration of Computer Execution Time

Table 13 gives in the case of the four foregoing cases the CDC 990 (NOS) seconds execution times for the various CORFEM calculations including the eigensolution checks together with the total number of inner loop iterations required. The table indicates that the execution times are minimal with about 0.15 cp seconds per iteration for the nine modes of the cases.

The IBM 3090 MVS/XA, rated at 50 million instructions per second, was used for the NASTRAN FEM analysis of a a 1326-SDOF wing model. The cp seconds for the important calculations are as follows:

(i) 60 to invert K_s of order 1326.

(ii) 4.5 to invert K_D of order 108.

(iii) 53 to calculate the B matrix.

(iv) 30 to calculate $B\,K_s B^t$ per element or

TABLE 9. FREQUENCY AND PERCENT ERROR CHANGES FOR CASE 2 USING 5 GVT MODES AND 5, 7, AND 9 FEM MODES (PASS 1 ONLY)

MODE NO.	GVT FREQ, HZ	INITIAL FEM		5 FEM MODES		7 FEM MODES		9 FEM MODES	
		FREQ, HZ	% ERROR	FREQ, HZ	% ERROR	FREQ, HZ	% ERROR	FREQ, HZ	% ERROR
1	7.562	9.097	20.3	7.550	-0.2	7.543	-0.3	7.523	-0.5
2	26.79	32.68	22.0	26.79	0.0	26.77	-0.1	26.67	-0.4
3	36.09	43.59	20.8	35.87	-0.6	35.99	-0.3	35.92	-0.5
4	77.64	94.74	22.0	78.22	-0.7	78.26	0.8	78.02	0.5
5	156.6	189.9	21.3	159.8	2.0	159.0	1.5	158.3	1.1
6	—	293.2	—	—	—	241.7	—	240.7	—
7	—	338.9	—	—	—	283.3	—	282.3	—
8	—	475.8	—	—	—	—	—	392.1	—
9	—	1826.	—	—	—	—	—	1530.0	—
FREQ. RMS ERROR		21.3%		1.01%		0.79%		0.64%	
SHAPE RMS ERROR		1.02%		0.57%		0.37%		0.40%	
NO. OF ITERATIONS		—		30		17		9	

TABLE 10. RESULTS OF CORRELATION WITH 7 GVT MODES USING 7 AND 9 FEM MODES FOR CASE 2 (PASS 1 ONLY)

ELEMENT NO.	ELEMENT TYPE	GVT GAGE	INITIAL FEM GAGE	INITIAL FEM % ERROR	7 FEM MODES GAGE	7 FEM MODES % ERROR	9 FEM MODES GAGE	9 FEM MODES % ERROR
1	S	.010	.015	50.0	0.01075	7.5	0.01063	6.3
2	M	.010	.015	50.0	0.00974	-2.6	0.00969	-3.1
3	S	.010	.015	50.0	0.01075	7.5	0.01058	5.8
4	M	.010	.015	50.0	0.01029	2.9	0.01045	4.5
5	S	.010	.015	50.0	0.01058	5.8	0.01062	6.2
6	S	.010	.015	50.0	0.01117	11.7	0.01064	6.4
7	S	.010	.015	50.0	0.01251	25.1	0.01191	19.1
8	M	.010	.015	50.0	0.00956	-4.4	0.00947	-5.3
9	M	.010	.015	50.0	0.01009	0.9	0.01003	0.3
10	S	.010	.015	50.0	0.01324	32.4	0.01310	31.0
11	M	.010	.015	50.0	0.01084	8.4	0.01094	9.4
12	S	.010	.015	50.0	0.01470	47.0	0.01473	47.3
13	S	.010	.015	50.0	0.01472	47.2	0.01477	47.7
14	S	.010	.015	50.0	0.01438	43.8	0.01413	41.3
15	M	.010	.015	50.0	0.01100	10.0	0.01104	10.4
S RMS ERROR			50.0%		30.4%		29.2%	
M RMS ERROR			50.0%		5.9%		6.5%	
FREQ. RMS ERROR			21.4%		0.31%		0.32%	
SHAPE RMS ERROR			0.93%		0.61%		0.63%	
NO. OF ITERATIONS			—		9		8	

S = SHEAR M = MEMBRANE

TABLE 11. RESULTS OF CORRELATION WITH 5 GVT MODES USING 5, 7, AND 9 FEM MODES FOR CASE 2 (PASS 1 ONLY)

ELEMENT NO.	ELEMENT TYPE	GVT GAGE	INITIAL FEM GAGE	INITIAL FEM % ERROR	5 FEM MODES GAGE	5 FEM MODES % ERROR	7 FEM MODES GAGE	7 FEM MODES % ERROR	9 FEM MODES GAGE	9 FEM MODES % ERROR
1	S	.010	.015	50.	0.01024	2.4	0.01039	3.9	0.01047	4.7
2	M	.010	.015	50.	0.01073	7.3	0.01023	2.3	0.01020	2.0
3	S	.010	.015	50.	0.01070	7.0	0.01063	6.3	0.01062	6.2
4	M	.010	.015	50.	0.01076	7.6	0.01080	8.0	0.01095	9.5
5	S	.010	.015	50.	0.01269	26.9	0.01141	14.1	0.01118	11.8
6	S	.010	.015	50.	0.01189	18.9	0.01153	15.3	0.01114	11.4
7	S	.010	.015	50.	0.01494	49.4	0.01330	33.0	0.01266	26.6
8	M	.010	.015	50.	0.01003	0.3	0.01019	1.9	0.01008	0.8
9	M	.010	.015	50.	0.01044	4.4	0.01031	3.1	0.01012	1.2
10	S	.010	.015	50.	0.01442	44.2	0.01350	35.0	0.01311	31.1
11	M	.010	.015	50.	0.01031	3.1	0.01054	5.4	0.01055	5.5
12	S	.010	.015	50.	0.01442	44.2	0.01408	40.8	0.01392	39.2
13	S	.010	.015	50.	0.01438	43.8	0.01409	40.9	0.01396	39.6
14	S	.010	.015	50.	0.01325	32.5	0.01354	35.4	0.01339	33.9
15	M	.010	.015	50.	0.01036	3.6	0.01080	8.0	0.01081	8.1
S RMS ERROR			50.0 %		34.1%		28.7%		26.4%	
M RMS ERROR			50.0 %		5.1%		5.4%		5.7%	
FREQ. RMS ERROR			21.3 %		1.01%		0.79%		0.64%	
SHAPE RMS ERROR			1.02%		0.57%		0.37%		0.40%	
NO. OF ITERATIONS			—		30		17		9	

S = SHEAR M = MEMBRANE

TABLE 12. RESULTS OF CORRELATION WITH 3 GVT MODES USING 5, 7, AND 9 FEM MODES FOR CASE 2 (PASS 1 ONLY)

ELEMENT NO.	ELEMENT TYPE	GVT GAGE	INITIAL FEM GAGE	INITIAL FEM % ERROR	5 FEM MODES GAGE	5 FEM MODES % ERROR	7 FEM MODES GAGE	7 FEM MODES % ERROR	9 FEM MODES GAGE	9 FEM MODES % ERROR
1	S	.010	.015	50.0	0.01199	19.9	0.01195	19.5	0.01194	19.4
2	M	.010	.015	50.0	0.01038	3.8	0.01042	4.2	0.01042	4.2
3	S	.010	.015	50.0	0.01127	12.7	0.01126	12.6	0.01126	12.6
4	M	.010	.015	50.0	0.01226	22.6	0.01217	21.7	0.01216	21.6
5	S	.010	.015	50.0	0.01353	35.3	0.01346	34.6	0.01345	34.5
6	S	.010	.015	50.0	0.01366	36.6	0.01362	36.2	0.01362	36.2
7	S	.010	.015	50.0	0.01383	38.3	0.01378	37.8	0.01377	37.7
8	M	.010	.015	50.0	0.01214	21.4	0.01202	20.2	0.01203	20.3
9	M	.010	.015	50.0	0.00969	3.1	0.00965	3.5	0.00965	3.5
10	S	.010	.015	50.0	0.01423	42.3	0.01418	41.8	0.01419	41.9
11	M	.010	.015	50.0	0.01001	0.1	0.01004	0.4	0.01005	0.5
12	S	.010	.015	50.0	0.01500	50.0	0.01500	50.0	0.01500	50.0
13	S	.010	.015	50.0	0.01497	49.7	0.01497	49.7	0.01498	49.8
14	S	.010	.015	50.0	0.01475	47.5	0.01466	46.6	0.01466	46.6
15	M	.010	.015	50.0	0.01046	4.6	0.01047	4.7	0.01047	4.7
S RMS ERROR			50.0%		38.9%		38.5%		38.5%	
M RMS ERROR			50.0%		13.0%		12.5%		12.5%	
FREQ. RMS ERROR			21.0%		1.46%		1.37%		1.37%	
SHAPE RMS ERROR			1.17%		0.48%		0.51%		0.51%	
NO. OF ITERATIONS			—		30		30		30	

S = SHEAR M = MEMBRANE

substructure, where generation of each K_s costs about 11 seconds.
See Eq. (A.9) of Appendix A.

The same model for 25 substructural elements, 108 DDOF, and 10 modes required 7 cp seconds to generate the generalized stiffness matrices and 1 cp second to calculate the derivatives on the CDC 990 (NOS/VE) computer.

Such costs can be extrapolated to develop a substructuring strategy, i.e., the number of substructures to be optimized. This is particularly important in the case of large structures because the optimization costs depend on the number of FEM passes, the number of unknowns to be optimized, the number of modes to correlate, and the foregoing cost breakdown.

TABLE 13. CDC 990 EXECUTION TIME

CASE	PASS 1 NO. ITER	PASS 1 TIME SEC	PASS 2 NO. ITER	PASS 2 TIME SEC	PASS 3 NO. ITER	PASS 3 TIME SEC	CHECK TIME SEC
1	6	1.9	6	2.6	—	—	0.6
2	8	2.6	12	2.8	—	—	0.6
3	25	4.8	10	2.6	8	2.8	0.6
4	1	1.3	—	—	—	—	—

6.0 Conclusions

A new and practical method (CORFEM) using first and higher order Van de Vooren perturbation formulae has been developed to efficiently and reliably correlate calculated frequencies and mode shapes with those of the corresponding measured natural modes by modifying the stiffness of the elements of the finite element model. The perturbation method effectively approximates the frequency and mode shape derivatives of each element and also the eigensolutions of the structure at the modal level. A gradient search algorithm modifies the elements within reasonable bounds and converges in incremental steps to an acceptable correlation. The eigensolution with the updated FEM verifies the results.

Both the analytical and test models of a wing torque box were generated using a NASTRAN coded structure to demonstrate CORFEM. Correlations were obtained for all nine modes of the system and for reduced numbers of modes. For the examples analyzed, the program converged to frequencies, mode shapes, and element gages within acceptable tolerances.

Because the Van de Vooren approach avoids complete FEM eigenvalue analysis to calculate frequency and mode shape derivatives and is more accurate than the Taylor series type linearization of constraints employed by conventional mathematical programming formulations, it application to large structures looks promising, notwithstanding the Virtual Work limitations and that the structure be statically determinate and internal load redistribution due to resizing or stiffness modification moderate. However, further work needs to be done to evaluate CORFEM for large FEM's and for actual test data. In addition, the effects of modifying the mass as well as the stiffness of the elements should be included in the method.

7.0 References

1. Baruch, M., "Correction of Stiffness Matrices Using Vibration Test," AIAA Journal, Vol. 20, No. 11, Nov. 1978, pp. 1623-1626.
2. Baruch, M., "Optimal Correction of Mass and Stiffness Matrices Using Measured Modes," AIAA Journal, Vol. 16, No. 11, Nov. 1982, pp. 1208-1210.
3. Baruh, H., and Meirovitch, L., "Parameter ID in Distribed Systems," Journal of Sound and Vibration, Vol. 101, 1985, pp 551-564.
4. Berman, A., " A Mass Matrix Correction Using an Incomplete Set of Measured Modes," AIAA Journal, Vol. 17, No. 10, Oct. 1985, pp 1147- 1148.
5. Creamer, N. G. and Junkins, J. L., "An Identification Method for Flexible Structures," AIAA Paper No. 87-0745, 1987.
6. Leuridan, J. M., Brown, D. L., and Allemang, R. T., "Direct System Parameter ID," 23rd AIAA Structures, Structural Dynamics and Materials Conference, AIAA Paper No. 82-762, 1982.
7. The NASTRAN Programmer's Manual (Level 17.5), National Aeronautics and Space Administration (NASA), Washington, D. C., NASA SP-223 (05), Dec. 1978; The NASTRAN User's Manual NASA SP-222(08), June 1986, COSMIC, University of Georgia, Athens, GA.
8. Van de Vooren, A. I., Report V.1366, "A Method to Determine the Change in Flutter Speed Due to Small Changes in the Mechanical System," National Aeronautical Research Institute, Amsterdam, 1947.
9. Wilkinson, K., Markowitz, J., Lerner, E., Chipman, R., George, D., et al, "An Automated Procedure for Flutter and Strength Analysis and Optimization of Aerospace Vehicles, FASTOP" Vol 1. Theory and Application, AFFDL-TR-75-137, Dec. 1975.
10. Gupta, V. K., and Marrujo, F. G., "Minimizing Unbalance Response of the CRBRP Sodium Pumps," Trans. 5th International Conference on Structural Mechanics in Reactor Technology (SMiRT), Paper F8/1, Aug. 1979; U.S. Dept. of Energy, Technical Review, Fall 1979, Clinch River Breeder Reactor Plant Report CRBRP-PMC 79-04.

APPENDIX A - DERIVATION OF COORDINATE TRANSFORMATION FROM DYNAMIC TO STRUCTURAL DOF

Let Q_S, K_S, and q_S be the structrual loads, stiffness matrix, and deflections in the global structural DOF system such that

$$Q_S = K_S q_S \tag{A.1}$$

The matrix K_S can be inverted to obtain:

$$q_S = K_S^{-1} Q_S \tag{A.2}$$

By means of an appropriate load distribution, T, a relationship between the structural and dynamic loads can be established, as follows:

$$Q_S = T Q_D \tag{A.3}$$

From the principle of equal work, the transpose of matrix T applies to the structural and dynamic deflections, q_S and q_D:

$$q_D = T^t q_S \tag{A.4}$$

Substitution of Eq. (A.3) into Eq. (A.2) and that result into Eq. (A.4) yields the dynamic flexibility matrix.

$$K_D^{-1} = T^t K_s^{-1} T \qquad (A.5)$$

The inverse of the dynamic flexibility matrix, K_D, can be expressed as follows:

$$Q_D = K_D q_D \qquad (A.6)$$

Substituting Eq. (A.3) and Eq. (A.6) into Eq. (A.2) yields an expression transforming the dynamic DOF to the structural DOF, as shown below:

$$q_s = K_s^{-1} T K_D q_D \qquad (A.7)$$

The transpose of the transformation matrix, B, is:

$$B^t = K_s^{-1} T K_D \qquad (A.8)$$

The structural mass and stiffness matrices, M_S and K_S, are transformed from the structural DOF to the dynamic DOF as follows:

$$M_D = B M_s B^t, \quad \text{and} \quad K_D = B K_s B^t \qquad (A.9)$$

APPENDIX B - ORTHOGONALIZATION OF MEASURED MODES

For a conservative system the summation of forces (ΣF) and moments (ΣMom) are zero. For the symmetric boundary conditions, these summations can be written in matrix form for the ith mode (V_i) of the test.

$$\Sigma F = \{1\}^t \left[\omega^2 M - K\right] \{V_i\} = 0 \qquad (B.1)$$

$$\Sigma Mom = \{x\}^t \left[\omega^2 M - K\right] \{V_i\} = 0 \qquad (B.2)$$

where M = mass matrix (may contain aeorodynamic forces)
K = stiffness matrix
ω = test mode frequency
x = longitudinal distances from reference axis to test points
{ } = column vector

Because of the inaccuracies in the raw data these conditions my not be met exactly. The reference axis of the rigid body modes is shifted to balance these equations.

Let $R = \left[\omega^2 M - K\right]$, then

$$\{1\}^t R (\{V_i\} + r_{1i} \{1\} + r_{2i} \{x\}) = 0 \qquad (B.3)$$

$$\{x\}^t R (\{V_i\} + r_{1i} \{1\} + r_{2i} \{x\}) = 0 \qquad (B.4)$$

The r's are unknown scalars that can be determined from the solution of the simultaneous Eq. (B.3) and Eq. (B.4) for each mode. The parenthesized terms on the left side of Eq. (B.3) and Eq. (B.4). represent the modified ith mode required to balance the forces and moments. If the change is small with respect to the original mode values (if a small shift in axis is computed), then the input data can be considered adequate for further processing.

The forces and moments to be balanced for the antisymmetric boundary conditions include the side forces, rolling moments, and yawing moments. These can be balanced in a similar fashion as the forces and moments of the symmetric case.

Having achieved the balance of forces and moments, the modes may next be orthogonalized. Vibrating structures can have an infinite number of natural modes which are said to be orthogonal with respect to a weighting function, the mass matrix of the structure. Orthogonal modes imply that the product of the forces in one mode and the displacements in another mode when summed up over the entire moving structure is zero. Expressed mathematically:

$$\int v_i v_j \, ds = 0 \qquad i \neq j \qquad (B.5)$$

where v_i = deflections in mode i
v_j = deflections in mode j
ds = incremental mass

In matrix form the orthogonality condition is expressible in terms of the generalized mass matrix, m_1.

$$[m_1] = V^t M V_1 \qquad (B.6)$$

The equations of motion using the generalized mass matrix can be written as:

$$q = \omega^2 \lambda_i [m_1]^{-1} [m_1] q \qquad (B.7)$$

where $[m_1]^{-1}$ = inverse of diagonal elements of $[m_1]$

λ_i = roots related to the test frequencies

ω = eigenvalue of the solution

If $[m_1]$ in Eq. (B.6) is diagonal with zero values for the off diagonal elements, the solution to Eq. (B.7) is trivial. However, because of experimental inaccuracies in measuring the mode shape, $[m_1]$ will not be exactly diagonal. The eigensolution to Eq. (B.7) will yield orthogonal modes which can be compared with the raw mode shapes and frequencies for consistency.

APPENDIX C - MODIFIED VAN DE VOOREN PERTURBATION METHOD

The basic harmonic equations of motion for a structural system are:

$$(K\lambda - G)\ v = 0 \qquad (C.1)$$

where K = square symmetric stiffness matrix
G = square symmetric matrix of mass terms plus aerodynamic terms, that may be complex and unsymmetric
λ = root or eigenvalue
v = mode shape or eigenvector

The solutions to Eq. (C.1) are Λ, a diagonal matrix of roots, and V, a square matrix of mode shapes, the ith column of which is associated with the ith value of λ_i.

The transposed set of equations to Eq. (C.1) are:

$$(K\lambda - G^t)\ u = 0 \qquad (C.2)$$

The solutions to Eq. (C.2) are Λ, the same roots as for Eq. (C.1), and U, a square matrix of mode shapes, the ith column of which is associated with the ith value of λ_i.

The biorthogonality conditions use the solution to Eq. (C.1) and (C.2) to give

$$(U^t K V\Lambda - U^t G V) = 0 \qquad (C.3)$$

$$(V^t K U\Lambda - V^t G^t U) = 0 \qquad (C.4)$$

Single out the jth mode of U and the ith mode of V, the

$$\{u_j\}^t K \{v_i\} \lambda_i - \{u_j\}^t G \{v_i\} = 0 \qquad (C.5)$$

$$\{v_i\}^t K \{u_j\} \lambda_j - \{v_i\}^t G \{u_j\} = 0 \qquad (C.6)$$

where { } = column vector

Subtract Eq. (C.6) from Eq. (C.5).

$$\{u_i\}^t K\{v_i\}\lambda_i - \{v_i\}^t K\{u_j\}\lambda_j =$$

$$\{u_j\}^t G\{v_i\} - \{v_i\}^t G\{u_j\} \qquad (C.7)$$

Note that the scalar results of the triple matrix products are equal.

$$\{u_j\}^t K\{v_i\} = \{v_i\}^t K\{u_j\} = a \qquad (C.8)$$

$$\{u_j\}^t G\{v_i\} = \{v_i\}^t G^t \{u_j\} = b \qquad (C.9)$$

Eq. (C.7) can be rewritten as follows:

$$a\,(\lambda_i - \lambda_j) = 0 \qquad (C.10)$$

For $i \neq j$, $a = 0$ and $b = 0$, since $(\lambda_i - \lambda_j) \neq 0$.

For $i = j$, $\lambda_i = b/a$, since $a \neq 0$ and $b \neq 0$.

Let $k = U^t KV$ and $g = U^t GV$, then k and g must be diagonal matrices.

Convert to the generalized coordinates (q).

$$v = V q \qquad (C.11)$$

Substitute Eq. (C.11) into Eq. (C.1) and premultiply by U^t.

$$(k\lambda - g)q = 0 \qquad (C.12)$$

From Eq. (C.5) $k = g\Lambda$, so that

$$k\,(\lambda - \Lambda)\,q = 0 \qquad (C.13)$$

The solutions to Eq. (C.13) yield the normal modes.

For $\lambda = \lambda_i$ $\quad q = \delta_{ij}$ $\quad \begin{cases} \delta_{ij} = 0 & i \neq j \\ \delta_{ij} = 1 & i = j \end{cases}$

where δ_{ij} = Kronecker's delta

Now apply the transformation of Eq. (C.11) to a change in stiffness (ΔK) and a change in the G matrix (ΔG).

Let $\alpha = U\,(\Delta G)V^t$ and $\beta = U\,(\Delta K)V^t$, then, from Eq. (C.13)

$$[k\,(\lambda - \Lambda) + \beta\lambda - \alpha]\,q = 0 \qquad (C.14)$$

The root and generalized mode solution for Eq. (C.14) for the ith mode are:

$$\left.\begin{aligned} \lambda &= \lambda_i + \Delta\lambda_i \\ q_{ji} &= \{\delta_{ji} + p_{ji}\} \end{aligned}\right\} \quad (C.15)$$

where $\Delta\lambda_i$ = change in λ_i

p_{ji} = change in generalized coordinate

By using a three mode set of equations, the perturbation solutions can be better visualized. The matrix Eq. (C.16) represents such a system including the changes in K and G, as an expansion of Eq. (C.14).

$$\begin{bmatrix} k_{11}-(\lambda-\lambda_1)+\beta_{11}\lambda-\alpha_{11} & \beta_{12}\lambda-\alpha_{12} & \beta_{13}\lambda-\alpha_{13} \\ \beta_{21}\lambda-\alpha_{21} & k_{22}-(\lambda-\lambda_2)+\beta_{22}\lambda-\alpha_{22} & \beta_{23}\lambda-\alpha_{23} \\ \beta_{31}\lambda-\alpha_{31} & \beta_{32}\lambda-\alpha_{32} & k_{33}-(\lambda-\lambda_3)+\beta_{33}\lambda-\alpha_{33} \end{bmatrix} \begin{Bmatrix} q_1 \\ q_2 \\ q_3 \end{Bmatrix} = 0 \quad (C.16)$$

Substitute the solutions of Eq. (C.14) into Eq. (C.16) to give three sets of matrix equations, one for each mode.

For mode 1: (C.17)

$$\begin{bmatrix} k_{11}-\Delta\lambda_1+\beta_{11}\gamma_1-\alpha_{11} & \beta_{12}\gamma_1-\alpha_{12} & \beta_{13}\gamma_1-\alpha_{13} \\ \beta_{21}\gamma_1-\alpha_{21} & k_{22}-(\gamma-\lambda)_2+\beta_{22}\gamma_1-\alpha_{22} & \beta_{23}\gamma_1-\alpha_{23} \\ \beta_{31}\gamma_1-\alpha_{31} & \beta_{32}\gamma_1-\alpha_{32} & k_{33}-(\gamma-\lambda)_3+\beta_{33}\gamma_1-\alpha_{33} \end{bmatrix} \begin{Bmatrix} 1 \\ p_{21} \\ p_{31} \end{Bmatrix} = 0$$

For mode 2: (C.18)

$$\begin{bmatrix} k_{11}-(\gamma-\lambda)_1+\beta_{11}\gamma_2-\alpha_{11} & \beta_{12}\gamma_2-\alpha_{12} & \beta_{13}\gamma_2-\alpha_{13} \\ \beta_{21}\gamma_2-\alpha_{21} & k_{22}-\Delta\lambda_2+\beta_{22}\gamma_2-\alpha_{22} & \beta_{23}\gamma_2-\alpha_{23} \\ \beta_{31}\gamma_2-\alpha_{31} & \beta_{32}\gamma_2-\alpha_{32} & k_{33}-(\gamma-\lambda)_3+\beta_{33}\gamma_2-\alpha_{33} \end{bmatrix} \begin{Bmatrix} p_{12} \\ 1 \\ p_{32} \end{Bmatrix} = 0$$

For mode 3: (C.19)

$$\begin{bmatrix} k_{11}-(\gamma-\lambda)_1+\beta_{11}\gamma_3-\alpha_{11} & \beta_{12}\gamma_3-\alpha_{12} & \beta_{13}\gamma_3-\alpha_{13} \\ \beta_{21}\gamma_3-\alpha_{21} & k_{22}-(\gamma-\lambda)_2+\beta_{22}\gamma_3-\alpha_{22} & \beta_{23}\gamma_3-\alpha_{23} \\ \beta_{21}\gamma_3-\alpha_{31} & \beta_{32}\gamma_3-\alpha_{31} & k_{33}-\Delta\lambda_3+\beta_{33}\gamma_3-\alpha_{33} \end{bmatrix} \begin{Bmatrix} p_{13} \\ p_{23} \\ 1 \end{Bmatrix} = 0$$

where $\gamma_1 = \lambda_1 + \Delta\lambda_1$, $\gamma_2 = \lambda_2 + \Delta\lambda_2$, $\gamma_3 = \lambda_3 + \Delta\lambda_3$

Assume a stiffness change only ($\alpha = 0$) and the mode shapes are orthonormalized (g=I), then to a first order of approximation (terms higher than first order are neglected), the general expression for change in the roots and generalized mode shapes are:

$$\left.\begin{aligned} \Delta\lambda_i &= -\lambda_i \beta_{ii} (k_{ii} + \beta_{ii})^{-1} \quad (C.20) \\ p_{ii} &= 1.0 \\ p_{ij} &= -\beta_{ij} (k_{ii} + \beta_{ii} - \gamma_j)^{-1} \end{aligned}\right\} \quad (C.21) \quad i \neq j$$

The γ of Eq. (C.21) uses the $\Delta\lambda$ of Eq. (C.20).

Two recursive methods are available for the second and higher order approximations. The general expression for the Recursive 1 method for changes in the roots and generalized mode shapes are found by using the implicit values for the roots to a previous order of approximation in the expanded Eq. (C.16), as follows:

$$(\Delta\lambda_i)_r = -(k_{ii} + \beta_{ii})^{-1} \left[\beta_{ii}\lambda_i + (\lambda_i)_\rho \sum_{j=1}^{n} \beta_{ij} (p_{ji})_\rho\right] \quad i \neq j \quad (C.22)$$

$$\left.\begin{aligned} p_{ii} &= 1.0 \\ (p_{ij})_r &= \\ &-\left[\beta_{ij} + \sum_{S=1}^{n} \beta_{iS} (p_{Sj})_\rho\right] \Big/ \left[k_{ii} + \beta_{ii} - (\lambda_i)_r\right]^{-1} \quad S \neq i,j;\ i \neq j \end{aligned}\right\} \quad (C.23)$$

where r = order of approximation
ρ = r-1
n = number of system modes

The Recursive 2 method for the second and higher order approximations uses the explicit expansion of Eq. (C.16) to yield the following expression for the second order of approximation:

$$(\Delta\lambda_i)_2 = -\lambda_i \Sigma \beta_{ij} p_{ji} / (k_{ii} + \Sigma \beta_{ij} p_{ji}) \quad i \neq j \quad (C.24)$$

The generalized mode shape calculations require the solution of a linear set of equations, one set for each mode. Although this procedure requires fewer iterations than for Recursive 1, the computer cost may be higher; and as shown in Table 1, there may be no need to proceed beyond the calculation of the second order approximation to the roots. Note in both recursive methods, the previous order roots and mode shapes are used for the next higher order, in order to accelerate convergence.

The first order Van de Vooren formulae were accurate enough to obtain derivatives of the frequencies and mode shapes in order to achieve convergence to a local minimum for the examples presented. Recursive 1 Van de Vooren formulae solutions are about 21 times more cost-effective than Jacobi method eigensolutions when solving all nine mass-orthonormal modes of the illustrative examples of Section 4.